Properties of Finite Nuclei*

K. S. MASTERSON, JR.†
University of California, San Diego, La Jolla, California
AND
A. M. LOCKETT
Los Alamos Scientific Laboratory, University of California, Los Alamos, New Mexico

(Received 20 August 1962)

The properties of Pb^{208} have been determined, using the Brueckner-Gammel-Weitzner theory of finite nuclei. Self-consistent solutions of the Hartree-Fock equations as modified by Brueckner and Goldman have been obtained. The properties computed include binding energy, mean proton and neutron radii, separation energies, spin-orbit splittings, nonlocal and state-dependent single-particle potentials, surface depth of density and potentials, and the potential-density relation. Semiquantitative agreement with experiment is obtained, the maximum difference between theory and experiment being of the order of 15%. Revised computations for Ca^{40} are reported to permit comparison between our results (with an improved treatment of the rearrangement energy) and those previously reported by Brueckner, Lockett, and Rotenberg for O^{16}, Ca^{40}, and Zr^{90}.

I. INTRODUCTION

IN a series of previous papers by Brueckner and coworkers,[1] methods have been developed for the study of many-fermion systems and have been applied in detail to the determination of the properties of nuclear matter. Approximate extensions of these methods to the study of finite nuclei were proposed by Brueckner, Gammel, and Weitzner,[2] and the properties of O^{16}, Ca^{40}, and Zr^{90} were calculated by Brueckner, Lockett, and Rotenberg.[3] The IBM 704 at Los Alamos, on which these computations were done, did not have the capacity to do the Pb^{208} calculation, and the problem was transferred to the CDC-1604 at the University of California, San Diego. A better approximation of the rearrangement energy was used. This paper reports the results of the numerical study of the properties of Pb^{208} and revised computations of Ca^{40} (to permit comparison with the previous calculations by BLR).

II. COMPUTATIONAL PROCEDURE

BGW and BLR discuss the procedure for extending the nuclear matter calculations of Brueckner and Gammel[1] to finite nuclei and examine the approximations involved. Therefore, we confine ourselves to stating briefly the pertinent equations, several of which have not previously been stated explicitly.

The problem is essentially that of solving the eigenvalue equation:

$$E_i\varphi_i(\mathbf{r})=\frac{p^2}{2m}\varphi_i(\mathbf{r})+\int d\mathbf{r}'\, V_i(\mathbf{r},\mathbf{r}')\varphi_i(\mathbf{r}') +V_R(r)\varphi_i(\mathbf{r}), \quad (2.1)$$

where $V_i(\mathbf{r},\mathbf{r}')$ is a nonlocal potential derived from the K matrices of the Brueckner theory and $V_R(r)$ is the rearrangement potential discussed and calculated by Brueckner and Goldman.[4]

The computational procedure consists of calculating a set of radial wave functions $R_{nlj}(r)$ from a Saxon well with approximately correct radius and depth. These wave functions are used to start the iteration procedure which consists of two separate parts, HI and HII. HI takes the wave functions and computes nonlocal potentials $V_{lj}(\mathbf{r},\mathbf{r}')$. From these potentials and the wave functions, $R_{nlj}(r)$, HII generates local equivalent potentials $F_{nlj}(r)$ and $G_{nlj}(r)$, and solves the Schrödinger equation for a new set of wave functions (using the iterative methods developed in BGW). The new wave functions are then used as input for the next iteration.

The nonlocal potential computed by HI is given by Eq. (94) of BGW:

$$\begin{aligned} V_{lj}(r_1,r_1')&=V_l^{(c)}(r_1,r_1')+\tfrac{1}{2}lV_l^{(LS)}(r_1,r_1'), \\ &\qquad j=l+\tfrac{1}{2}, \quad l\geq 0 \\ &=V_l^{(c)}(r_1,r_1')-\tfrac{1}{2}(l+1)V_l^{(LS)}(r_1,r_1'), \\ &\qquad j=l-\tfrac{1}{2}, \quad l>0, \end{aligned} \quad (2.2)$$

where, by Eq. (4.17) of BLR

$$\begin{aligned} V_l^{(c)}(r_1,r_1')&=\frac{1}{2}\int_{-1}^{1} d\mu\, P_l(\mu)(\mathbf{r}_1|\,V^{(c)}\,|\mathbf{r}_1') \\ &=\frac{1}{2}\int_{|r_1-r_1'|}^{r_1+r_1'}\frac{xdx}{r_1r_1'}P_l(\hat{r}_1\cdot\hat{r}_1')(\mathbf{r}_1|\,V^{(c)}\,|\mathbf{r}_1'), \end{aligned} \quad (2.3)$$

with $\mu=\hat{r}_1\cdot\hat{r}_1'$ and $\mathbf{x}=\mathbf{r}_1'-\mathbf{r}_1$ (see Fig. 1). $V^{(LS)}(\mathbf{r}_1,\mathbf{r}_1')$ is given by a similar equation. $V_0(r,r')$ is graphed in Fig. 2(a) for $r=1.0$ F.

We trace the integral (2.3) back to the K matrices tabulated in BGW or to an appropriate Born approximation as follows:

* This work was done in part under the auspices of the U. S. Atomic Energy Commission.

† Lieutenant, U. S. Navy, on duty under instruction at the University of California.

[1] See K. A. Brueckner and J. L. Gammel, Phys. Rev. **109**, 1023 (1958), for a list of references.

[2] K. A. Brueckner, J. L. Gammel, and H. Weitzner, Phys. Rev. **110**, 431 (1958), hereafter referred to as BGW.

[3] K. A. Brueckner, A. M. Lockett, and M. Rotenberg, Phys. Rev. **121**, 255 (1961), hereafter referred to as BLR.

[4] K. A. Brueckner and D. T. Goldman, Phys. Rev. **116**, 424 (1959); **117**, 207 (1960).

(1) $(\mathbf{r}_1|V|\mathbf{r}_1')$ is expanded in Legendre polynomials, and the first two terms are retained [Eq. (4.9) of BLR]:

$$(\mathbf{r}_1|V|\mathbf{r}_1')=(\mathbf{r}_1|V|\mathbf{r}_1+\mathbf{x}) \simeq V_0(r_1,x)+V_1(r_1,x)\cos(\mathbf{r}_1,\mathbf{x}), \quad (2.4)$$

where V_0 and V_1 are obtained by evaluating $(\mathbf{r}_1|V|\mathbf{r}_1+\mathbf{x})$ for $\mathbf{x}$ parallel and antiparallel to $\mathbf{r}_1$:

$$\begin{aligned} V_0(r_1,x)&=\tfrac{1}{2}[(\mathbf{r}_1|V|\mathbf{r}_1+x\hat{r}_1)+(\mathbf{r}_1|V|\mathbf{r}_1-x\hat{r}_1)] \\ V_1(r_1,x)&=\tfrac{1}{2}[(\mathbf{r}_1|V|\mathbf{r}_1+x\mathbf{r}_1)-(\mathbf{r}_1|V|\mathbf{r}_1-x\mathbf{r}_1)]. \end{aligned} \quad (2.5)$$

(2) In general, $(\mathbf{r}_1|V|\mathbf{r}_1')$ is given by an equation of the form

$$(\mathbf{r}_1|V|\mathbf{r}_1')=\int d\mathbf{r}_2 d\mathbf{r}_2'\varphi^*(\mathbf{r}_2)(\mathbf{r}_{12}|K|\mathbf{r}_{12}')\varphi(\mathbf{r}_2') \times\delta^3\left(\frac{\mathbf{r}_1+\mathbf{r}_2}{2}-\frac{\mathbf{r}_1'+\mathbf{r}_2'}{2}\right), \quad (2.6)$$

[Eqs. (77) and (78) of BGW]. The $(\mathbf{r}_{12}|K|\mathbf{r}_{12}')$ are the matrix elements tabulated in BGW. The delta function expresses the conservation of center of mass implicit in the assumption (discussed in BGW) that the K matrices have a negligible dependence on the total momentum. It is apparent that $\mathbf{r}_1$, $\mathbf{r}_1'$, $\mathbf{r}_2$, and $\mathbf{r}_2'$ must form a parallelogram (Fig. 1).

(3) After performing the r_2' integration, one obtains for the terms on the right of Eq. (2.5)

$$\begin{aligned} &V_N^{(c)}(\mathbf{r}_1,\mathbf{r}_1\pm x\hat{r}_1) \\ &=16\pi\int_0^\infty r_{12}^2 dr_{12}\int_{|r_{12}-2x|}^{r_{12}+2x}\frac{r_{12}'dr_{12}'}{2xr_{12}}\{\tfrac{1}{2}H_N(\mathbf{r}_2,\mathbf{r}_2')_\pm \\ &\times[(r_{12}|K|r_{12}')_{s,e}+3(r_{12}|K|r_{12'})_{t,\,o,\,\text{central}}] \\ &+\tfrac{1}{4}H_P(\mathbf{r}_2,\mathbf{r}_2')_\pm[(r_{12}|K|r_{12}')_{s,e} \\ &+3(r_{12}|K|r_{12}')_{t,\,o,\,\text{central}}+(r_{12}|K|r_{12}')_{s,o} \\ &+3(r_{12}|K|r_{12}')_{t,\,o,\,\text{central}}]\}, \end{aligned} \quad (2.7)$$

and

$$\begin{aligned} &V_N^{(LS)}(\mathbf{r}_1,\mathbf{r}_1\pm x\hat{r}_1) \\ &=16\pi\int_0^\infty r_{12}^2 dr_{12}\int_{|r_{12}-2x|}^{r_{12}+2x}\frac{r_{12}'dr_{12}}{2xr_{12}}\left(1-\frac{\mathbf{r}_1\cdot\mathbf{r}_2}{r_1^2}\right) \\ &\times\{\tfrac{3}{2}H_N(\mathbf{r}_2,\mathbf{r}_2')_\pm(r_{12}|K|r_{12}')_{t,o,LS}+\tfrac{3}{4}H_P(\mathbf{r}_2,\mathbf{r}_2')_\pm \\ &\times[(r_{12}|K|r_{12}')_{t,e,LS}+(r_{12}|K|r_{12}')_{t,o,LS}]\}. \end{aligned} \quad (2.8)$$

The proton potentials are given by similar equations with H_N and H_P (the density matrix elements) interchanged. These equations are derived in BGW [Eqs. (89) and (90)] and in BLR [Eq. (4.15)]. The factor 16π comes from the ϕ integration and the delta function in Eq. (2.6). Note that $\mathbf{r}_2$ and $\mathbf{r}_2'$ appearing above are determined by $\mathbf{r}_1$, $\mathbf{r}_1'$ and the variables of integration, including x and the sign with which it appears in the terms on the left. We have appended the subscript "$\pm$" on H_N and H_P to indicate this dependence. The density matrix elements are defined by Eqs. (85), (86), and (87) of BGW:

$$H_N(\mathbf{r}_2,\mathbf{r}_2')=\sum_{nlj}\frac{R_{nlj}(r_2)R_{nlj}(r_2')N_{nlj}}{4\pi r_2 r_2'}P_l^0(\mathbf{r}_2,\mathbf{r}_2'), \quad (2.9)$$

with a similar equation for H_P. N_{nlj} is the occupation number for the state ($2j+1$ for full shells).

(4) In the computations, the even state K-matrix elements were used for the S and D states in the following combination:

$$(r_{12}|K|r_{12}')_{s,e} =\sum_{l=0,2}(2l+1)(r_{12}|K_l|r_{12}')_{s,e}P_l(\mathbf{r}_{12},\mathbf{r}_{12}'), \quad (2.10)$$

with a similar equation for $(r_{12}|K|r_{12}')_{t,e}$. For the D states, a local equivalent potential was calculated by hand from the BGW K-matrix elements (see BLR for the reason and justification for this). The odd-state central and tensor potentials were not included: They cancel each other almost completely. As discussed in BLR, the even spin-orbit term in Eq. (2.8) was also dropped (its experimental justification being questionable). For the odd-state spin-orbit contribution in Eq.

TABLE I. Parameters of the Gammel-Thaler potentials. The potentials all have the Yukawa form outside of a repulsive core of radius 0.4 F.

State	Strength, V (MeV)	Inverse range, μ (F^{-1})
Triplet central even	− 877.39	2.0908
Tensor even	− 159.40	1.0494
Spin-orbit even	−5000	3.70
Singlet even	− 434.0	1.45
Triplet central odd	− 14.0	1.00
Tensor odd	22.0	0.80
Spin-orbit odd	−7315	3.70
Singlet odd	130.0	1.00

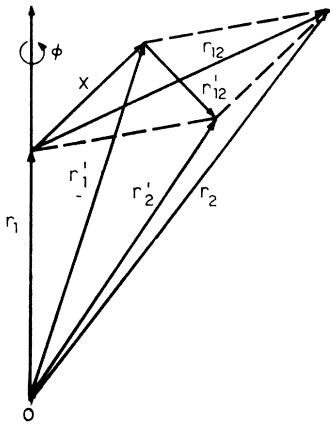

FIG. 1. Relationships between variables in the theory of finite nuclei.

(2.8), and for the even-state terms outside the nonlocal region (e.g., outside the range of the tables in BGW), the Born approximation was used. The Born terms were calculated from the potentials in Table I, and for S and D states they are

$$(r_{12}|K|r_{12}')=V(r_{12}')\delta(r_{12}'-r_{12})/4\pi r_{12}r_{12}', \quad (2.11)$$

where, in terms of the parameters of Table I, $V(r)$ is of the form

$$V(r)=Ve^{-\mu r}/\mu r. \quad (2.12)$$

For the spin-orbit term, we obtain (using only the P-state contribution):

$$V_N^{(LS)}(\mathbf{r}_1,\mathbf{r}_1\pm x\hat{r}_1)$$
$$=16\pi\int_0^\infty r_{12}^2dr_{12}\int_{|r_{12}-2x|}^{r_{12}+2x}(\pm g)\frac{r_{12}'dr_{12}'}{2xr_{12}}$$
$$\times[\tfrac{3}{2}H_N(\mathbf{r}_2,\mathbf{r}_2')_\pm+\tfrac{3}{4}H_p(\mathbf{r}_2,\mathbf{r}_2')_\pm]3P_1(\mathbf{r}_{12},\mathbf{r}_{12}')$$
$$\times\frac{\delta(r_{12}-r_{12}')}{4\pi r_{12}^2}V_{t,o}^{(LS)}\frac{e^{-\mu_{t,o}^{(LS)}r_{12}'}}{\mu_{t,o}^{(LS)}r_{12}'}. \quad (2.13)$$

The factor g is an approximation to the $(1-\mathbf{r}_1\cdot\mathbf{r}_2/r_1^2)$ term in Eq. (2.8). The appropriate expression is obtained by expanding $H(\mathbf{r}_2,\mathbf{r}_2')$ about $\mathbf{r}_1$ and ignoring derivatives higher than the first (which is justified by the near locality of the spin-orbit K matrix), and then by averaging over the angles which occur in the subsequent integrations. This procedure leads to

$$g=\tfrac{1}{3}(r_{12}/r_1)\cos(\mathbf{x},\mathbf{r}_{12})(1-2r_{12}^2/x). \quad (2.14)$$

This approximation reduces to the Thomas expression if $V^{(LS)}$ is independent of l. The corresponding proton potential is obtained by interchanging H_N and H_P in Eq. (2.13).

(5) The core contribution, as computed from Eqs. (54) and (56) of BGW, is

$$(r_c|K|r_c)=A\frac{\delta(r_{12}-r_c)\delta(r_{12}'-r_c)}{4\pi r_c^2}\frac{(1-b/1.07)}{(1-b/r_0)}, \quad (2.15)$$

with $A=215$ or 257 MeV-F and $b=0.488$ or 0.459 F for singlet or triplet states, respectively, and

$$r_0=[3/4\pi\rho(r)]^{1/3}. \quad (2.16)$$

The density, $\rho(r)$, is the diagonal element of the total density matrix, e.g., $H_N(\mathbf{r},\mathbf{r})+H_P(\mathbf{r},\mathbf{r})$.

Because of the magnitude of the problem of computing the nonlocal potential for Pb^{208}, some modification of the order of integration from that of BLR was necessary. For a given value of all the variables of integration, the appropriate terms were calculated for $r_1'=r_1+x$ and $r_1'=r_1-x$. Then the r_{12}' and r_{12} integrations were performed, the r_{12}' integration being inside the r_{12} integration. The x integration was then done for all values of r_1' simultaneously; e.g., for each point in the x integral, the terms were computed for every value of r_1'. This sequence was repeated for each of the 50 r_{12} points. The total time for this phase of the computation was 70 min. The meshes were (in fermis):

r_1	50 points	0.2 (0.2) 10.0
r_1'	125 points	−1.55 (0.025) 1.55
x	43 points	0.0 (0.05) 2.1
r_{12}	13 points	0.4 (0.1) 1.0 (0.3) 1.6 (0.5) 3.6
r_{12}'	17 points	$(r_{12}-0.60)$ (0.05) $(r_{12}+0.20)$.

An intermediate step between HI and HII was required for the lead calculation. The nonlocal potentials were generated by HI and stored on magnetic tape as four matrices (neutron and protons, $j=l\pm\frac{1}{2}$) of dimension 7×125 (l,r') for each of the 50 values of r (here we change notation from r_1 to r and r_1' to r'). The intermediate code reordered these records on magnetic tape to 22 sets of $V_{lj}(r,r')$ in the order in which HII treated each state. [Of the 38 states involved in this calculation, 16 differ from some other proton or neutron state only in the principal quantum number, n, and thus have the same $V_{lj}(r,r')$.] This intermediate operation took 15 min.

Two calculations were performed by HII. The first calculation was of the potential functions F and G [Eqs. (4.24) and (4.25) of BLR]:

$$F_{nlj}(r)=4\pi r\int r'dr'\frac{V_{lj}(r,r')}{D_{nlj}(r)}\Big[R_{nlj}(r')R_{nlj}(r)$$
$$+a^2\frac{dR_{nlj}(r')}{dr'}\frac{dR_{nlj}(r)}{dr}\Big]+V_c(r), \quad (2.17)$$

and

$$G_{nlj}(r)=4\pi a^2r\int r'dr'\frac{V_{lj}(r,r')}{D_{nlj}(r)}$$
$$\times\Big[R_{nlj}(r')\frac{dR_{nlj}(r)}{dr}-R_{nlj}(r)\frac{dR_{nlj}(r')}{dr'}\Big], \quad (2.18)$$

where

$$D_{nlj}(r)=[R_{nlj}(r)]^2+a^2[dR_{nlj}(r)/dr]^2, \quad (2.19)$$

and $V_c(r)$ is the coulomb potential. The constant a was chosen to be 1 F (the order of the range of the nonlocality of $V(r,r')$), as in BLR. Representative potential functions $F(r)$ and $G(r)$ and radial wave functions, $R(r)$, are plotted in Fig. 2.

A simple iterative method for solving the radial eigenvalue equation derived from Eq. (2.1) is described by BGW. It leads to an equation for the $(n+1)$st iterate of the radial wave function $R_{nlj}(r)$ in terms of the nth iterate values of the $F(r)$ and $G(r)$ given by Eqs. (2.17) and (2.18):

$$(E_i-H_0)(R^{n+1}(r)/r)=[F^n(r)+V_R(r)][R^{n+1}(r)/r]$$
$$+[G^n(r)/r][dR^{n+1}(r)/dr]. \quad (2.20)$$

We have used an improved approximation to the rearrangement potential, $V_R(r)$, which is suggested by the analysis of Brueckner and Goldman,[4] who determined the dependence of the rearrangement potential on the single particle momentum (as a fraction of p_F). In BLR, $V_R(r)$ was approximated as a constant factor

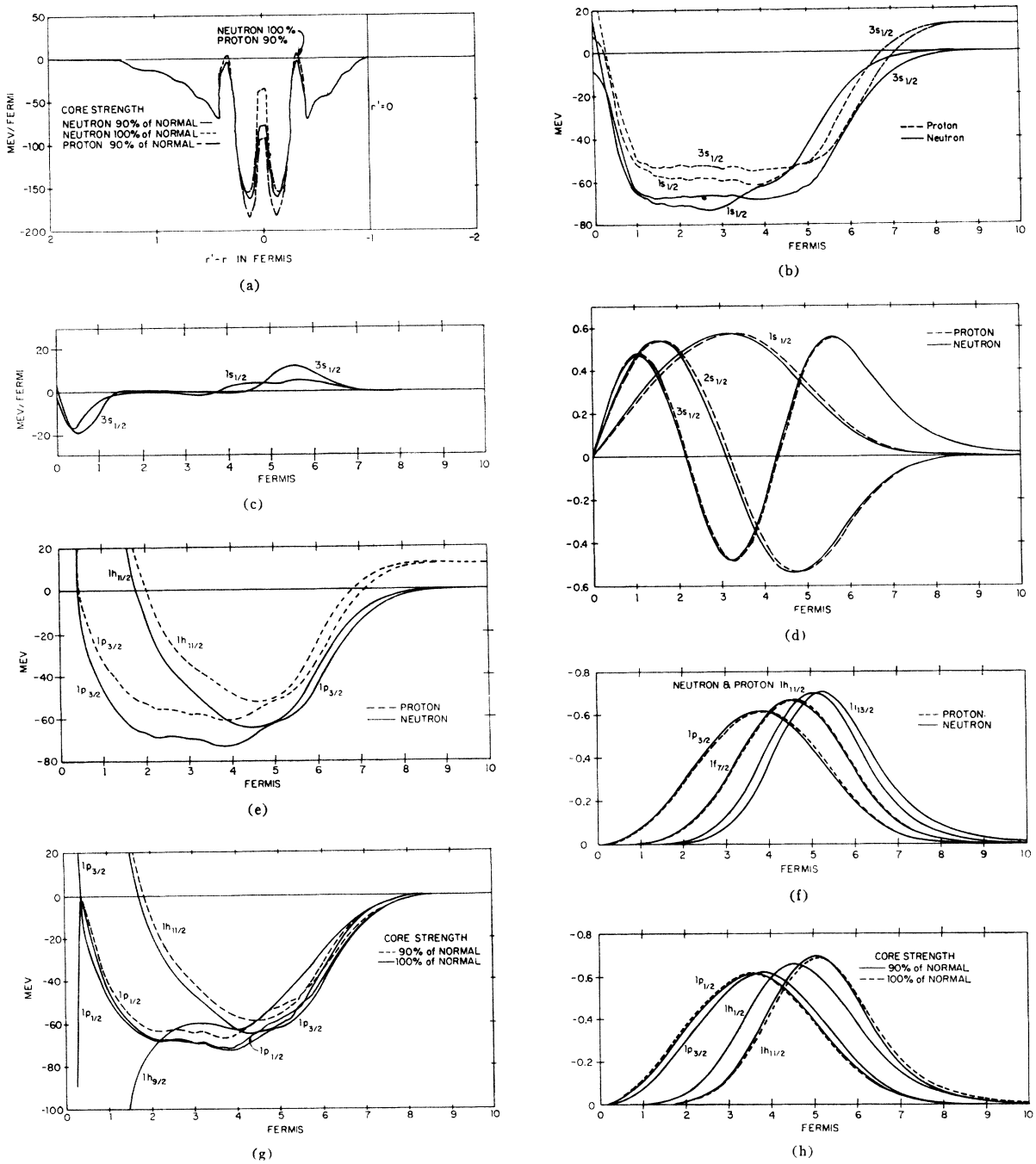

FIG. 2. Representative potential and wave functions for Pb^{208}. (a) Nonlocal potential, $4\pi rr'V(r,r')$ for $r=1.00$ F, illustrating variation with strength of hard core potential (90 and 100% of normal) and differences between neutron and proton potentials; (b) Potential function $F(r)$ for s states, indicating the variation with principal quantum number and differences between neutron and proton functions; (c) Potential function $G(r)$ for s-state neutrons, indicating dependence on principal quantum number; (d) Radial wave functions, $R(r)$, for the s-state protons and neutrons; (e) Potential function $F(r)$ for neutrons and protons for two representative states; (f) Radial wave functions, $R(r)$, for neutrons and protons for selected states illustrating the variation with orbital quantum number; (g) Potential function $F(r)$ for both core strengths for selected states illustrating the spin-orbit splitting; (h) Radial wave functions corresponding to the potential functions of 2(g). Unless otherwise indicated, all data are for core strength 90% of normal.

TABLE II. Properties of Ca^{40} calculated with the new rearrangement energy approximation (this paper) compared to the previous calculations of BLR and to experiment. Energies are in MeV, distances in F.

Property	Calculated value: This paper	Calculated value: Previous (BLR)	Experimental value
Separation energy			
neutron	−12.6	−13.5	−15.63
proton	− 5.5	− 4.9	− 8.34
difference	− 7.1	− 8.6	− 7.29
Total energy per particle	− 6.55	− 6.12	− 8.55
Rms radii			
total	2.99	2.88	
neutron	2.98	2.84	
proton	3.00	2.91	3.52±0.07
Spin-orbit splitting			
$1p_{1/2}$–$1p_{3/2}$			
neutron	3.6	6.1	
proton	3.5	5.9	
$1d_{3/2}$–$1d_{5/2}$			
neutron	4.9	7.1	
proton	4.8	6.7	

times $[\rho(r)]^2$. Our new approximation is

$$V_R(r) = \{26-14[(E_{nlj}{}^{N \text{ or } P}-E_{\text{bottom}})/(E_{\text{top}}-E_{\text{bottom}})]\} \times[\rho(r)/\rho(r_0=1.07)]^2. \quad (2.21)$$

$\rho(r_0=1.07)=0.19488$ particles/F^3. This equation interpolates in terms of the energy eigenvalues between the rearrangement energy corresponding to the approximate mean momentum of the deepest state and the energy appropriate to the top state (e.g., between 26 and 12 MeV, respectively, at normal density). This improved treatment of the rearrangement energy is the only essential difference between our calculation and that of BLR.

The solution of Eq. (2.20) is discussed in detail in BLR. The procedure starts with choosing an appropriate trial eigenvalue and doing a Runga-Kutta integration out from the origin to an intermediate radius, R_{test}, and in from a very large radius to R_{test}. The latter integration starts with the logarithmic derivative of $R_{nlj}(r)$ set equal to that of the appropriate asymptotic solution of the Schrödinger equation. This integration is done with successively better estimates of the eigenvalues until the logarithmic derivatives of the wave functions match at R_{test}. The wave functions are then normalized to unity. The entire HII calculation had to be repeated three or four times per iteration to obtain satisfactory convergence. This minor iteration procedure took about 25 min, ten of which were required for calculating the F and G.

The total energy per particle quoted in the next section (and in BLR) is given by

$$E_{\text{total per particle}}=E_{\text{total}}/(\text{number of particles}), \quad (2.22)$$

where

$$E_{\text{total}}=\sum_{\substack{i \text{ all} \\ \text{particles}}}\left\{E_i-\int dr\left[R_i^2(r)(\tfrac{1}{2}F_i(r)+V_R(r)) +\tfrac{1}{2}R_i(r)G_i(r)\frac{dR_i(r)}{dr}\right]\right\}, \quad (2.23)$$

a result which is easily derived.

III. RESULTS

A. Comparison with Previous Rearrangement Energy Approximation

In order to check our revised code and to ascertain the effects of the new treatment of the rearrangement energy, we calculated the properties of Ca^{40} and compared our results with the original code used by BLR at Los Alamos, both with and without the new energy treatment. The agreement between the BLR code and our code was good: −6.78 vs −6.55 MeV mean energy per particle, 3.00 vs 2.99 F rms radii, and 0.7 MeV or less difference in the eigenvalues. The differences are entirely attributable to a few minor coding errors in the original program. Table II compares the new results with those reported in BLR. The net effect of our improved rearrangement energy approximation is slightly better agreement with experiment for almost every property tabulated: separation energies, total energy per particle, and rms radii. In addition, the spin-orbit splittings are more nearly proportional to the $(2l+1)$ separations generally expected. However, the magnitude of the total energy per particle is still not large enough (−6.55 MeV vs the experimental −8.55 MeV),[5] the proton rms radius is too small (although it is increased by 3% to a new value which is 83% of the experimental value),[6] and there is slightly too much difference between the separation energy of the last particle and the total energy per particle (1.1 MeV compared to the previous 1.2 MeV and the experimental 0.2 MeV). Comparative potential energies and eigenvalues are given in Table III for every state of Ca^{40} with the old and new approximations. The range of eigenvalues has been reduced from −70.1 through −4.9 MeV to −48.7 through −5.5 MeV. This reduction in spread of energies indicates that the previous approximation reproduced the absolute magnitudes of the energy spectrum quite poorly except near the top levels; the otherwise close agreement between the two calculations indicates that the approximation employed in BLR was adequate for the computation of the average properties of the nuclei (such as mean energies, rms radii, etc), and that

[5] The experimental energies quoted in this paper are calculated from experimental masses tabulated by L. A. König, J. H. E. Mattauch, and A. H. Wapstra, Nucl. Phys. **31**, 18 (1962).

[6] The proton radii and surface depths quoted in this paper are the electron scattering values summarized by R. Hofstadter, Rev. Mod. Phys. **28**, 214 (1956), and by D. G. Ravenhall, *ibid.* **30**, 430 (1958).

TABLE III. Calculated potential energies and eigenvalues for Ca^{40} with the new approximation to the rearrangement energy (this paper) and with the previous approximation (BLR). The core strength was 90% of the normal value. All energies are in MeV.

	This paper				Previous calculation (BLR)			
	Potential energy		Eigenvalue		Potential energy		Eigenvalue	
State	Neutron	Proton	Neutron	Proton	Neutron	Proton	Neutron	Proton
$1s_{1/2}$	−58.4	−51.1	−48.7	−41.4	−82.4	−72.1	−70.1	−60.0
$1p_{3/2}$	−51.4	−44.1	−34.0	−26.7	−65.2	−55.1	−44.7	−35.1
$1p_{1/2}$	−48.5	−41.1	−30.4	−23.2	−59.3	−49.3	−38.6	−29.2
$1d_{5/2}$	−43.0	−35.5	−17.5	−10.3	−48.3	−38.2	−20.6	−11.6
$2s_{1/2}$	−38.1	−30.2	−14.8	− 7.6	−40.5	−30.0	−16.0	− 7.3
$1d_{3/2}$	−37.9	−30.3	−12.6	− 5.5	−39.6	−29.6	−13.5	− 4.9

further improvement in this direction would not be likely to change such properties appreciably.

B. General Properties of Pb^{208}

In Table IV we tabulate the principal properties of Pb^{208} as calculated by the theory for hard-core strengths equal to 90% and 100% of the normal strength. The 100% core data is the result of a single full iteration from the 90% data. Experience with the rapid convergence of these computations indicates that the properties tabulated are very near the values we would obtain with further iteration (e.g., probably within 0.1 MeV for the mean energy and 0.01 F for the rms radii). Since the individual energy-level predictions (next section) are subject to slight fluctuations on the first iterations, they are not quoted for the full core. The 90% core was chosen to permit comparison with the calculations in BLR. In those calculations, the reduced core contributions were arbitrarily employed as a means of improving the binding energies. As we see in Table V, too little binding was obtained for the smaller nuclei even with the reduced core strength. However, for lead with the 90% core the binding energies of the last particles are a fraction of an MeV too great (−8.8 vs −8.4 MeV for the top neutron and −8.9 vs −8.0 MeV for the proton), and the magnitude of the total energy per particle (10.0 MeV) is 2.1 MeV greater than that calculated from the masses. The energy of the top nucleon differs by 1.2 MeV from the total energy per particle, compared with the experimental value of 0.5 MeV. For the 100% core, the magnitude of the total energy per particle is several MeV less than the energy with the 90% core, and is 1 MeV less than the experimental value.

The rms proton radii are 16 and 15% too small (for the 90 and 100% cores, respectively). Similar errors were reported for Ca^{40} and Zr^{90}. The surface depths are 1.8 and 1.9 F for the proton distributions and 1.9 and 2.1 F for the total distributions. (We have taken the surface depth to be the distance over which the density falls from 90 to 10% of its maximum value in the vicinity of the center of the nucleus.) The computed depths are slightly smaller than the experimentally deduced (2.2±0.3) F for the charge distribution[6] and ($2.45_{-0.15}^{+0.45}$) F for the nuclear distribution.[7] The small discrepancies might vanish with the correction of the error in the rms radii.

C. Energy Spectrum

Table VI gives the energy spectrum for the reduced (90%) hard core strength. The ordering of states is generally in accord with that deduced from experiment for the shell model.[8] Up through the $1g_{9/2}$ state, the Pb^{208} level assignment is the same as that calculated for Zr^{90} (and differs from the Ca^{40} order in the $1d_{3/2}$ and $2s_{1/2}$ states). With the new rearrangement energy treatment, the spread in energy levels and the coarse level spacing are probably the most accurate calculated to date. Thus, we compare our spread in eigenvalues of about 70 MeV with those determined in the shell-model calculations with central potentials and spin-orbit coupling of (for example) Malenka[9] (about 30 MeV) and of Ross, Mark, and Lawson[10] (less than 40 MeV). In

TABLE IV. Properties of Pb^{208} calculated for core repulsion strengths 90% and 100% of normal values. Energies are in MeV and distances in F.

	Calculated		Experimental
	90% core	100% core	
Separation energy or top eigenvalue			
neutron	−8.8		−7.38
proton	−8.9		−8.04
difference	+0.1		+0.66
Total energy per particle	−10.00	−6.86	−7.87
Total rms radius	4.67	4.75	
neutron radius	4.74	4.84	
proton radius	4.56	4.62	5.42±0.11
Surface depth			
total	1.9	2.1	$2.45^{+0.45}_{-0.15}$
neutron	1.9	2.3	
proton	1.8	1.9	2.2 ±0.3

[7] L. R. B. Elton, Rev. Mod. Phys. **30**, 557 (1958).
[8] M. G. Mayer and J. H. D. Jensen, *Elementary Theory of Nuclear Shell Structure* (John Wiley & Sons, Inc., New York, 1956).
[9] B. J. Malenka, Phys. Rev. **86**, 68 (1952).
[10] A. A. Ross, Hans Mark, and R. D. Lawson, Phys. Rev. **102**, 1613 (1956).

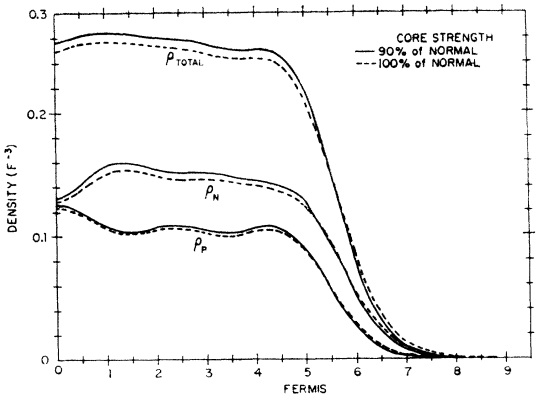

FIG. 3. Proton, neutron, and total densities for repulsive core strengths equal to 90 and 100% of normal values.

general, their relative spacing of low-lying levels is in good agreement with ours. However, both authors obtain a level sequence at the surface which differs from ours: For instance, for neutrons, Ross *et al.* have $3p_{1/2}$, $3p_{3/2}$, $2f_{5/2}$, $1i_{13/2}$, $\cdots$ compared to our $3p_{1/2}$, $1i_{13/2}$, $2f_{5/2}$, $3p_{3/2}$, $\cdots$; and, for protons, they have $3s_{1/2}$, $2d_{3/2}$, $1h_{11/2}$, $\cdots$ compared to our $1h_{11/2}$, $3s_{1/2}$, $2d_{3/2}$, $\cdots$. In both cases, the spread of energies is less than 2 MeV. The above differences can be traced to the spin-orbit potential, which is imperfectly known and which is treated as a parameter in the shell-model calculations to improve agreement with experiment.

The spin-orbit splittings for the various states are tabulated in Table VII. They are of the right order of magnitude and follow in a reasonable manner the expected $(2l+1)$ graduation in magnitude. In Figs. 2(g) and 2(h) we have indicated the dependence of the local equivalent potential, $F(r)$, and of the wave functions on this splitting. In particular, we note an appreciable spatial splitting of levels with the same orbital angular momentum but with opposite spin.

D. Neutron-Proton Density Relations

The neutron, proton, and total density distributions are indicated in Fig. 3 for the two core strengths. We note the remarkably uniform total density, and the moderate nonuniformity of the neutron and proton contributions. We also see that the neutron and proton wave functions [Figs. 2(d) and 2(f)] are almost identical for corresponding states, with the exception of a very slight shift towards the center of the nucleus in the low angular momentum states. Thus, much of the difference in the density distributions is due to the "extra" neutrons in the outer energy shell (which are distributed throughout the nucleus as well as at the surface). We find that the neutron-proton radii differ by about 0.2 F, extending to the larger nuclei the tendency noted in BLR for the proton and neutron distributions to have nearly equal radii. The origin of this effect lies in the symmetry energy and in the insensitivity of the wave functions to differences in potential. The absence of an

TABLE V. Recapitulation of results for O^{16}, Ca^{40}, and Zr^{90} with the old arrangement energy (V_R) approximation and results of this paper for Ca^{40} and Pb^{208} with the new rearrangement energy approximation, Eq. (2.21).

Element	Core strength	V_R	E_{av} Calc.	E_{av} Exp.	R_{rms} Calc.	R_{rms} Exp.
O^{16}	1.00	old	−2.02	−7.98	2.58	2.57 ±0.05
	0.825	old	−4.41		2.41	
Ca^{40}	1.00	old	−3.89	−8.55	3.07	3.52 ±0.07
	0.90	old	−6.12		2.91	
	0.90	new	−6.55		3.00	
Zr^{90}	1.00	old	unbound	−8.71	···	~4.24
	0.90	old	−5.80		3.56	
Pb^{208}	1.00	new	−6.86	−7.87	4.62	5.42 ±0.11
	0.90	new	−10.00		4.56	

TABLE VI. Calculated potential energies and eigenvalues for Pb^{208} for core strength 90% of the normal value. All energies are in MeV.

State	Potential energy Neutron	Potential energy Proton	Eigenvalue Neutron	Eigenvalue Proton
$1s_{1/2}$	−70.3	−58.4	−65.9	−54.1
$1p_{3/2}$	−68.6	−56.7	−59.7	−48.0
$1p_{1/2}$	−67.9	−56.1	−58.4	−47.0
$1d_{5/2}$	−65.9	−54.1	−51.7	−40.1
$1d_{3/2}$	−65.2	−53.3	−49.7	−38.3
$2s_{1/2}$	−64.1	−51.5	−47.5	−35.2
$1f_{7/2}$	−62.6	−50.8	−42.5	−30.8
$1f_{5/2}$	−62.0	−49.9	−39.5	−28.1
$2p_{3/2}$	−59.4	−47.0	−36.8	−24.4
$2p_{1/2}$	−59.7	−47.1	−34.7	−22.7
$1g_{9/2}$	−59.0	−47.0	−32.2	−20.3
$1g_{7/2}$	−58.3	−46.0	−28.0	−16.5
$2d_{5/2}$	−53.3	−41.2	−25.2	−12.7
$2d_{3/2}$	−55.5	−42.6	−22.6	−10.4
$3s_{1/2}$	−52.4	−39.8	−22.5	− 9.7
$1h_{11/2}$	−54.8	−42.9	−21.1	− 8.9
$1h_{9/2}$	−54.0		−15.6	
$2f_{7/2}$	−45.5		−13.5	
$3p_{3/2}$	−41.9		−10.9	
$2f_{5/2}$	−49.9		−10.3	
$1i_{13/2}$	−50.2		− 9.2	
$3p_{1/2}$	−45.0		− 8.8	

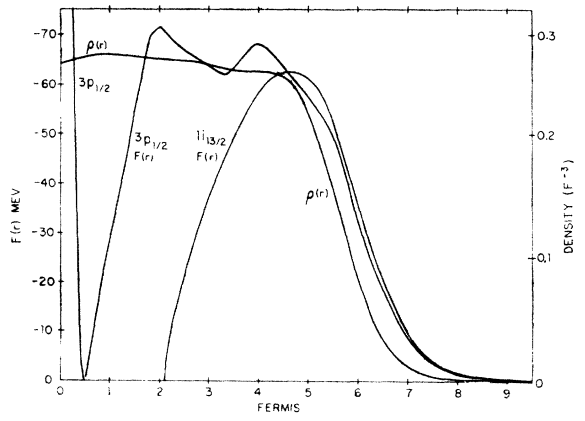

FIG. 4. $F(r)$ for the highest two neutron states of Pb^{208} and the total density as a function of radius. The core strength was 90% of normal.

appreciable neutron-proton difference for the light nuclei (BLR) and the slight difference noted for lead are compatible with experimental results.[11] Quantitatively, for lead we conclude from pion and nucleon scattering calculations[7] that $R_N-R_p=(0.2\pm0.2)$ F, where R is the half-density radius, in agreement with our calculation. This figure does not include that part of the difference which results from the finite extension of the nuclear potential beyond the matter distribution when the radii are determined from separate nuclear and charge-dependent interactions. We discuss this difference next.

E. Density-Potential Relations

In Fig. 4 we have plotted the potential function $F(r)$ for the two top neutron states against the density distribution. The top proton potential is not shown because it lies inside the neutron potentials, a consequence of the smaller proton distribution. The separation between total density and potential (0.5 F) is slightly less than that of Ca^{40} and Zr^{90} (0.75 F); the difference between the proton half-density point and the nuclear potential half-maximum is 0.7 F. These results agree within the limits of experimental error with the differences between $R_P=(1.18\pm0.02)\,A^{1/3}=(7.00\pm0.14)$ F from electron scattering[6,12] and from μ mesonic atoms,[13] and $R_V=(1.25\pm0.05)\,A^{1/3}=(7.41\pm0.30)$ F from low and high energy neutron scattering.[14] Wilets[15] has concluded from neutron and proton scattering that the difference between the nuclear potential radius and the matter radius is independent of A and is (1.0 ± 0.3) F. This difference in radii is largely due to three effects previously discussed,[16] namely, (a) finite range of interaction; (b) nonlinear variation of potential energy with density (Wilets effect)[17]; and (c) nonlocality of the effective interaction.

F. Comparison with Surface Predictions of Other Theories

It is interesting to compare the character of the nuclear surface as predicted by previous semiempirical theories with our results (which are essentially from "first principles" if the concept of a two-body nuclear potential is valid). We will mention only two previous calculations to indicate the degree of precision obtainable. One is the pure Hartree-Fock calculation by Rotenberg[18] with $N=Z=92$. It yielded surface thicknesses of 2.7 and 3.1 F for Gaussian and Yukawa wells, respectively, and predicted a marked dip in the proton distribution near the origin (which is absent in our more exact calculation). The calculated separation between the rms radii of the particle density and of the self-consistent collective potential in this model was less than 0.2 F. An intermediate step between the pure Hartree-Fock calculation and the BGW theory is the semiempirical model of Berg and Wilets.[15,17] This model yields $R_N-R_P=0.2$ F (in agreement with our result) and $R(\text{potential})-R(\text{nucleon})=0.7$ F (compared to our 0.5 F).

TABLE VII. Spin-orbit splitting for Pb^{208} in MeV. The core strength was 90% of its normal value.

	Neutron	Proton
$1p_{1/2}-1p_{3/2}$	1.3	1.0
$2p_{1/2}-2p_{3/2}$	2.1	1.7
$3p_{1/2}-3p_{3/2}$	2.1	
$1d_{3/2}-1d_{5/2}$	2.0	1.8
$2d_{3/2}-2d_{5/2}$	2.6	2.3
$1f_{5/2}-1f_{7/2}$	3.0	2.7
$2f_{5/2}-2f_{7/2}$	3.2	
$1g_{7/2}-1g_{9/2}$	4.2	3.8
$1h_{9/2}-1h_{11/2}$	5.5	

G. Summary of Results for the Four Nuclei Studied to Date

The following is a summary of the general features of the results for full-shell nuclei (O^{16}, Ca^{40}, Zr^{90} and Pb^{208}) studied in this paper and in BLR.

(1) The magnitudes of the total energy per particle and of the separation energies are smaller than their experimental counterparts.

(2) The difference between observed and calculated energies decreases with increasing nuclear size.

(3) The energy spectrum is in general agreement with experiment, and the computation of the coarse spacing, with the new rearrangement energy approximation, is probably the most accurate to date. However, the detailed spacing between close levels, particularly when widely different angular momenta are involved, may not be correct in every instance.

(4) The energy spectrum is quite sensitive to any changes in the calculation (as, for example, the changes in the treatment of the rearrangement energy and in the core strength). This is to be expected, because the single-particle energies are to be compared with potential wells of the order of 70 MeV. Thus, a MeV change in particle energy is less than a 2% change in potential energy.

(5) The radii of the nucleon distributions are in good agreement with experiment for O^{16}, with full core, but are about 15% too small for the other nuclei studied.

(6) These radii are relatively insensitive to changes

[11] W. N. Hess and B. J. Moyer, Phys. Rev. **101**, 337 (1955); R. W. Williams, *ibid.* **98**, 1387 (1955).
[12] K. W. Ford and D. L. Hill, Ann. Rev. Nucl. Sci. **5**, 25 (1955).
[13] E. M. Henley, Rev. Mod. Phys. **30**, 438 (1958).
[14] S. Fernbach, Rev. Mod. Phys. **30**, 414 (1958); J. H. Atkinson, W. N. Hess, V. Perez-Mendez, and R. Wallace, Phys. Rev. **123**, 1850 (1961).
[15] L. Wilets, Rev. Mod. Phys. **30**, 542 (1958).
[16] K. A. Brueckner, Phys. Rev. **103**, 1121 (1956); Rev. Mod. Phys. **30**, 561 (1958).
[17] R. A. Berg and L. Wilets, Phys. Rev. **101**, 201 (1956); L. Wilets, *ibid.* **101**, 1805 (1956).
[18] M. Rotenberg, Phys. Rev. **100**, 439 (1955).

in the calculation, a "stiffness" which has been observed in the calculations of BLR and of this paper.

(7) The theory predicts the details of the internal density distribution, and the calculations have brought out a remarkably uniform ratio of neutron and proton densities in the lighter nuclei, with only minor variance in Pb^{208}. To date it has not been possible to verify the detailed internal distributions of these nuclei experimentally, although the analysis of Ford and Hill[12] indicates that the charge distribution for lead is probably reasonably uniform (and especially that there is no dip in the center as deduced for gold),[6] in agreement with our results.

(8) The calculated surface properties are compatible with present experimental evidence. In particular, the surface depth, neutron-proton radius differences, and the matter-potential relations at the surface are quantitatively predicted.

IV. CONCLUSIONS

The surface depth of the nucleus is now known experimentally to within about 10%.[6] Our results are compatible with experiment and form a theoretical explanation of its shape from first principles. Indeed, there is a need for further refinement of the experiment to verify the internal structure of each nucleus and to ascertain the surface shape consistent with it. There is also a need for further refinement of the BGW theory to obtain better rms radii, with the result that the surface depths predicted might be more accurate. In addition, our theoretical knowledge of the neutron and proton density ratios and of the potential-density relation at the surface is compatible with, and at present more definitive than, experiment. A feature of the surface which this theory does not describe is possible existence (discussed by Wilkinson)[19] of nucleon clusters, possibly "alpha" particles, in the nuclear surface. Superfluidity in the low-density region, if present, is also not treated, but it is believed to have negligible effect on a gross property such as surface depth.

For the remaining properties (binding energy, mean proton and neutron radii, separation energies, and spin-orbit splittings), the theory is in semiquantitative agreement with experiment, the maximum errors being of the order of 15%. The sources of these errors can be grouped into three categories: (1) the numerical procedures, (2) the input (i.e., the phenomenological potentials), and (3) the theory itself (both the Brueckner theory of infinite nuclear matter and the BGW theory of finite nuclei). The first of these (the numerical procedures) is rejected as a source of major error on the basis of the thorough tests by BLR of the meshes employed and the improvement of the results with nuclear size in spite of the fact that any errors from the numerical procedures probably increased also.

However, some of the error may arise in the choice of the phenomenological two-body nuclear potential. Recent calculations[20] of the properties of nuclear matter show that different phenomenological potentials which apparently give "equally good" fit to scattering data do not necessarily lead to identical nuclear properties for the many-body system. It is possible that a better potential would resolve some of the discrepancies between our calculations and experiment. It should be noted that of the seven potentials employed in the calculations of reference,[20] the potential of Table I gives the best agreement between the calculated and semiempirical properties of infinite nuclear matter. This, however, does not mean that this potential is the "correct" one, and more work in phenomenological potentials is indicated. Further, in the more accurate calculations of Brueckner and Gammel[1] this potential yielded for nuclear matter a slightly smaller binding energy (−15.2 MeV) than the semiempirical value (best value −15.8 MeV, but values from −15.5 to −17.0 are also quoted)[21] and an equilibrium spacing that was 5% too small (1.02 vs 1.07 F). These effects undoubtedly influence the computations of BLR and of this paper. In addition, there is some question whether the hard core should be nearer 0.4 F (as in the Gammel–Thaler potential we use) or 0.5 F (as suggested by more recent determinations of phenomenological potentials).[22] A potential with a larger core might give lower density saturation and larger nuclear radii.

The improvement with increasing mass number of the computed binding energy strongly suggests that the principal source of error is in the treatment of the "surface" energy, which is considerably too large. It should be emphasized that the "surface" energy, in our calculations, does not arise solely from the classical effect related to the density variation in the surface. The rearrangement energy, which is essential in the finite system in the determination of the wave function and density, and hence indirectly in the determination of the total energy, does not appear in the uniform system. Thus, its effect in the finite nucleus is, in fact, a "surface" effect. The methods of BLR and of this paper are at best a treatment of the rearrangement problem based on plausibility; they are not rigorously proved. Further investigations of this many-body problem peculiar to the finite system are clearly needed.

In conclusion, we have ascertained that the BGW theory of finite nuclei is in semiquantitative agreement with experiment, the agreement improving with nuclear size. Further, we have seen that our state-dependent

[19] D. H. Wilkinson, *Proceedings of the International Conference on Nuclear Structure, Kingston, Canada* (University of Toronto Press, Toronto, 1960), p. 20.

[20] K. A. Brueckner and K. S. Masterson, Jr., Phys. Rev. **128**, 2267 (1962).

[21] A. E. S. Green, Rev. Mod. Phys. **30**, 569 (1958); A. G. W. Cameron, Can. J. Phys. **35**, 1021 (1957).

[22] K. E. Lassila, M. H. Hull, Jr., H. M. Ruppel, F. A. McDonald, and G. Breit, Phys. Rev. **126**, 881 (1962).

approximation to the rearrangement energy correction gives appreciably better results than those obtained in the previous calculations. Finally, it appears probable that much of the residual error in the results can be removed by improvements in the phenomenological two-body potential upon which the calculations are based, and by improvement of the "surface" energy.

ACKNOWLEDGMENTS

We wish to acknowledge the cooperation and assistance of the computation facility of the University of California, San Diego (directed by Dr. C. L. Perry). We also wish to thank Dr. K. A. Brueckner for his support and many helpful discussions during the progress of the calculations.

PHYSICAL REVIEW VOLUME 129, NUMBER 2 15 JANUARY 1963

He^3+t Reactions*†

DARRYL B. SMITH, NELSON JARMIE, AND A. M. LOCKETT

Los Alamos Scientific Laboratory, University of California, Los Alamos, New Mexico

(Received 20 August 1962)

The energy distributions of alpha particles and of protons from the He^3+t reactions have been measured for 1.9-MeV incident tritons at laboratory angles of 30° for alphas, and both 30° and 90° for protons. Absolute cross sections are obtained. The spectra are discussed in terms of a model which assumes that uncorrelated three-body breakup and several two-stage processes all contribute independently to the cross section. The calculations based on this model are in excellent agreement with the observed spectral shapes. The neutron-proton correlation corresponding to the unbound singlet state of the deuteron is observed. The binding energy of He^5 (for breakup into a neutron and an alpha particle) was found to be $\epsilon=-0.79\pm0.03$ MeV.

INTRODUCTION

RECENTLY, there has been considerable interest in the interpretations of reactions of the type

$$a+A\rightarrow b+c+d.$$

Each of the three particles in the final state has a spectrum of energies. The shape of the spectrum depends on the nuclear forces acting in the system and for this reason has not yet been derived exactly. Nevertheless, such reactions as $d+p\rightarrow p+p+n$, $d+n\rightarrow p+n+n$, $t+d\rightarrow t+p+n$, $\alpha+d\rightarrow\alpha+p+n$, $t+t\rightarrow\alpha+n+n$, $Be^9+p\rightarrow\alpha+\alpha+d$, $K^-+p\rightarrow\bar{K}^0+\pi^-+p$, and $\Sigma^-+d\rightarrow$ (Λ^0 or Σ^0)$+n+n$[1-6,8-11] are often discussed in terms of the cluster model which suggests that three-body decay can be treated as a time sequence of two-body interactions[4-7] or in terms of final-state interactions among the reaction products.[8-15]

The $T(t,\alpha)n,n$ reaction for triton energies below 2.1 MeV has been investigated in some detail at this laboratory,[6] and the alpha-particle energy spectra were fairly well explained by a two-stage process calculation. The present experiment is a similar study of the $He^3(t,\alpha)p,n$ reaction.

When helium-3 is bombarded with tritium, the following reactions are the only ones possible at low bombarding energies:

$$He^3+t\rightarrow He^4+d, \quad (Q=14.320 \text{ MeV}) \quad (1)$$

$$\rightarrow He^5+p\rightarrow\alpha+p+n, \quad (Q=11.14 \text{ MeV}) \quad (2)$$

$$\rightarrow Li^5+n\rightarrow\alpha+p+n, \quad (Q=10.13 \text{ MeV}) \quad (3)$$

* Work performed under the auspices of the U. S. Atomic Energy Commission.

† This work represents part of a thesis prepared in partial fulfillment of the requirements for the degree of Master of Science at the University of New Mexico.

[1] L. Cranberg and R. K. Smith, Phys. Rev. **113**, 587 (1959).

[2] C. Werntz and H. Lefevre (to be published).

[3] M. P. Nakada, J. D. Anderson, C. C. Gardner, J. McClure, and C. Wong, Phys. Rev. **110**, 594 (1958); C. Wong, J. D. Anderson, C. C. Gardner, J. W. McClure, and M. P. Nakada, *ibid.* **116**, 164 (1959).

[4] M. Alston, L. W. Alvarez, P. Eberhard, M. L. Good, W. Graziano, H. K. Ticho, and S. G. Wojcicki, Phys. Rev. Letters **6**, 300 (1961); S. Minami, Progr. Theoret. Phys. (Kyoto) **26**, 356 (1961).

[5] E. H. Beckner, C. M. Jones, and G. C. Phillips, Phys. Rev. **123**, 255 (1961).

[6] N. Jarmie and R. C. Allen, Phys. Rev. **111**, 1121 (1958).

[7] G. C. Phillips, T. A. Griffy, and L. C. Biedenharn, Nucl. Phys. **21**, 327 (1960).

[8] N. A. Vlasov, S. P. Kalinin, B. V. Rybakov, and V. A. Sidorov, J. Exptl. Theoret. Phys. (U.S.S.R.) **38**, 1733 (1960) [translation: Soviet Phys.—JETP **11**, 1251 (1960)]; B. V. Rybakov, V. A. Sidorov, and N. A. Vlasov, Nucl. Phys. **23**, 491 (1961).

[9] K. Ilakovac, L. G. Kuo, M. Petravic, I. Slaus, and P. Tomas, Phys. Rev. Letters **6**, 356 (1961).

[10] W. Heckrotte and M. MacGregor, Phys. Rev. **111**, 593 (1958).

[11] Y. Y. Chen, Nuovo Cimento **19**, 36 (1961).

[12] K. M. Watson, Phys. Rev. **88**, 1163 (1952).

[13] A. B. Migdal, J. Exptl. Theoret. Phys. (U.S.S.R.) **28**, 3 (1955) [translation: Soviet Phys.—JETP **1**, 2 (1955)].

[14] V. V. Komarov and A. M. Popova, J. Exptl. Theoret. Phys. (U.S.S.R.) **38**, 253 (1960) [translation: Soviet Phys.—JETP **11**, 184 (1960)]; *ibid.*, p. 1559 [translation, *ibid.*, p. 1123]; Nucl. Phys. **18**, 296 (1960); Akad. Nauk. S.S.S.R., Izvestiia Ser. Fiz. (English translation) **24**, 1154 (1960).

[15] J. E. Young, Phys. Rev. **116**, 1201 (1959).